X-ray free-electron lasers development

Claudio Pellegrini

UCLA Department of Physics and Astronomy

SLAC National Accelerator Laboratory

Outline

- Introduction to X-ray Lasers and X-ray free-electron lasers (FELs)

- The physics and present status of X-ray FELs

- The science being done at LCLS

- Future developments

Why X-ray lasers?

A laser generating high intensity, coherent X-ray pulses at Ångstrom wavelength and femtosecond pulse duration -the characteristics time and space scale for atomic and molecular phenomena- allows imaging of periodic and non periodic systems, non crystalline states, studies of dynamical processes in systems far from equilibrium, nonlinear science, opening a new window on atomic and molecular phenomena of interest to biology, chemistry, material sciences and physics.

**SLAC** Time scales: smaller systems, shorter times. Atomic scale, 1Å, time fs ⟶ X-ray FEL

UCLA

the technology gap
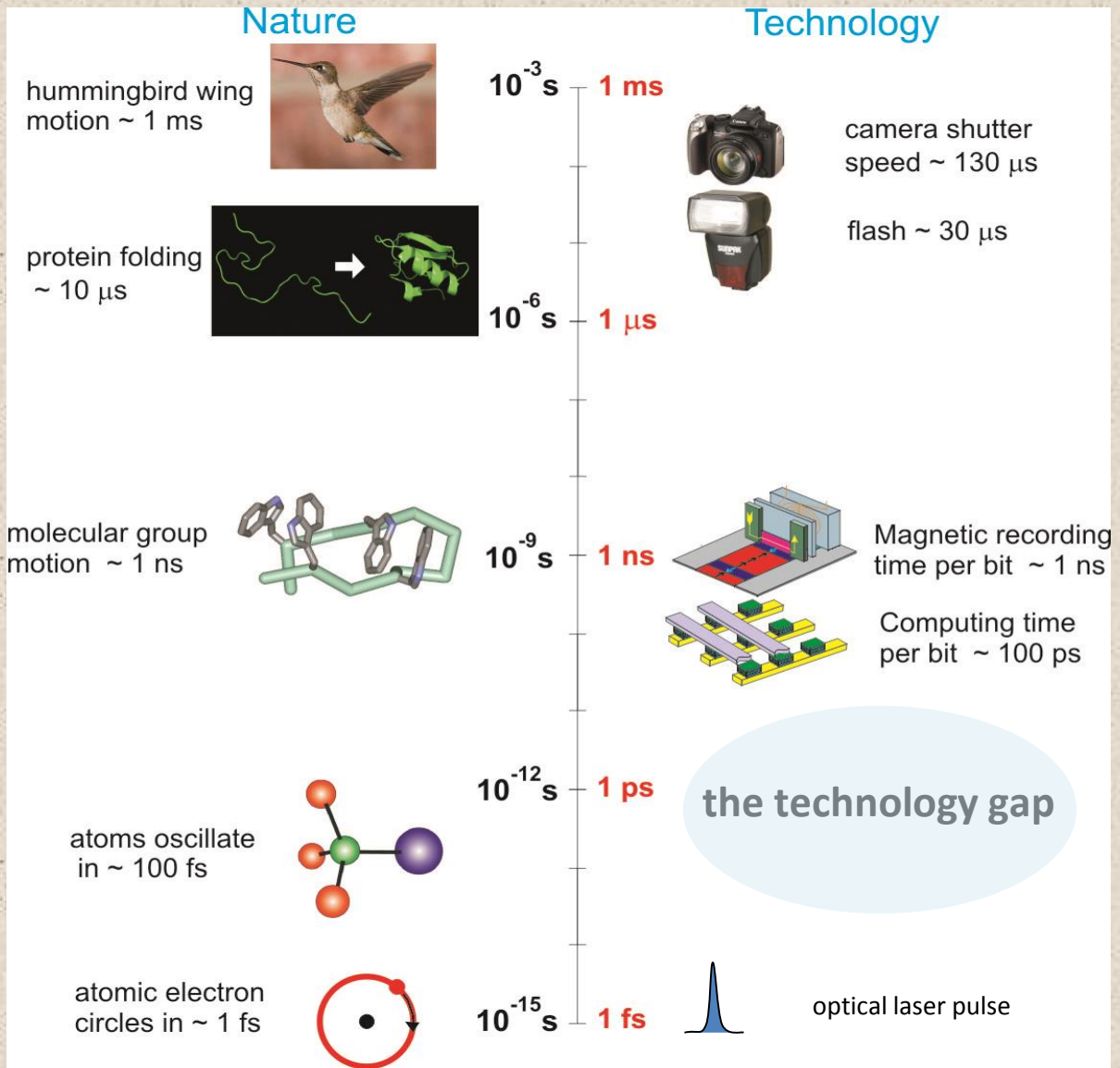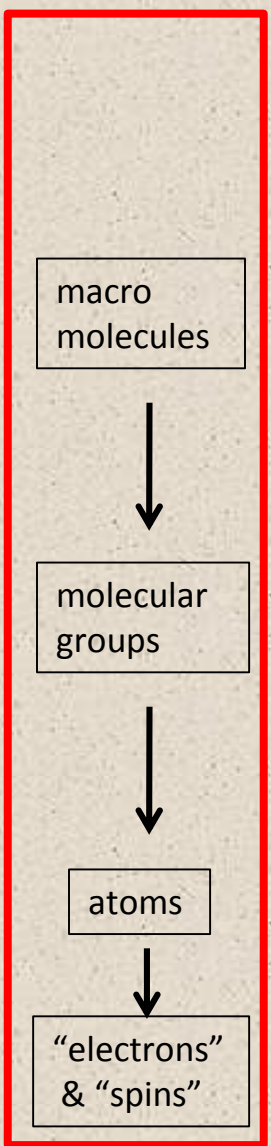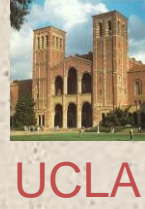
Courtesy J. Stohr

Early work on X-ray lasers

1960: A breakthrough, first laser light
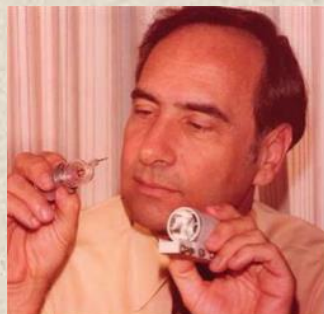
Ted Maiman (25 years
after first Ruby laser)
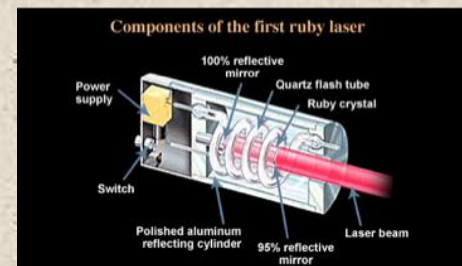
The interest in X-ray lasers started in the 70's, following the first infrared laser in 1960. In the atom-based, population inversion, laser approach, reaching the X-ray wavelength is extremely difficult, because of the very short lifetime of excited atom-core inner quantum energy levels. George Chapline and Lowell Wood of Lawrence Livermore National Laboratory estimated the radiative lifetime of an X-ray laser transition would be about 1 fs times the square of the wavelength in angstroms.(Chapline G. and L. Wood,1975, Physics Today **40**, 8).

The short lifetime and large energy needed to excite inner atomic levels, 1 to 10 KeV compared to about 1 eV for visible lasers, lead to a very intense pumping power requirement to attain population inversion, too large for practical purposes. Building low loss optical cavities for X-ray laser oscillators is also difficult.

Early work on X-ray lasers
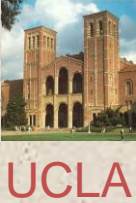
But not to be discouraged: Scientists at LLNL proposed to use a nuclear weapon to drive an X-ray laser. They tried the concept in the Dauphin experiment, apparently with success, in 1980.(Hecht J., 2008, The History of the X-ray Laser, Optics and Photonics News, 19 (2008)).

During the Cold War X-ray lasers were supposed to be used to destroy incoming missiles. *Joseph Nilsen, "Legacy of the X-ray Laser Program," Lawrence Livermore National Laboratory Report, also Energy and Tech. Rev. Nov. 1994*

High peak power, short pulse, visible light lasers made possible another approach: pumping cylindrical plasmas, in some cases confining the plasma with magnetic fields. These experiments led to X-ray lasing around 18 nm with gain of about 100 in1985 (Matthews D.L. et al., 1985, Physics Review Letters **54**, 110, Suckewer S. et al., 1985, Physics Review Letters **55**, 1753.) From that time lasing has been demonstrated, with limited peak power and tunability, at several wavelengths in the soft X-ray region. A review of the most recent developments with this approach is given in*Suckewer S. and P. Jaeglé, 2009, Laser Physics Letters **1**, 411 (2009)

An alternative solution

The way out of this difficult situation is given by self amplified spontaneous emission free-electron laser (SASE FEL), generating X-rays from high brightness relativistic electron beams.

A proposal in 1992 (*C. Pellegrini, 1992 Proc. of the Workshop on 4th generation light sources, SSRL/SLAC Rep. 92/02*) to build an X-ray FEL using 1 km of the SLAC linac, producing a 15GeV high brightness beam, lead to the design and construction of LCLS at SLAC. In 2009 LCLS successfully started to work (*P. Emma et al., 2010 Nat. Phot. 4, 641*) with characteristics similar or better than originally proposed.

A history of this development is found in C. *Pellegrini, X-ray free-electron lasers: from dreams to reality, Physica Scripta T169, 014004 (2016).*
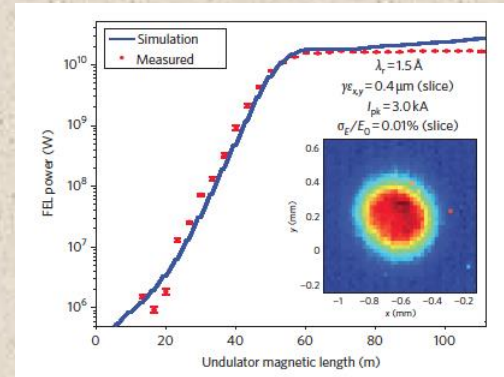
LCLS saturates: 1.5 Å, 4/2009, 1-3 mJ.
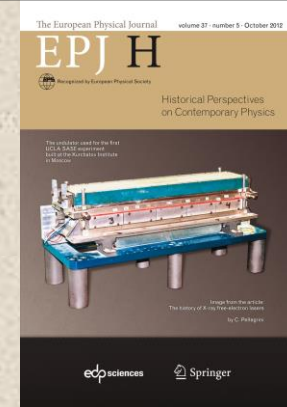
60 cm long undulator used for the first 16 μm SASE FEL at UCLA . *Varfolomeev, A.A. et al., 1992 Nucl. Instr. and Meth. A 318, 813.*

The alternative solution

Population inversion doesn't work for an X-ray laser. How does the X-ray FEL work?

1. Use undulator radiation from relativistic electrons.

2. Generate an electron beam with electrons squeezed in micro-bunches $\lambda/10$ long and separated by λ, a kind of 1-D relativistic crystal. Intensity proportional to electron number $N_e^{1+\alpha}$, $\alpha=1$ for a perfect crystal, $0<\alpha\leq1$ for non perfect case.

3. How do we do it? We do not have an electron gun capable of generating such a beam, and it would be hard to imagine one at 1A wavelength.

4. Solution: use a collective instability* to do it for us.

*Bonifacio R., Pellegrini C., Narducci L., COLLECTIVE INSTABILITIES AND HIGH-GAIN REGIME IN A FREE ELECTRON LASER, 1984 Optics Comm. **50**, 373.

UCLA

Undulator Radiation
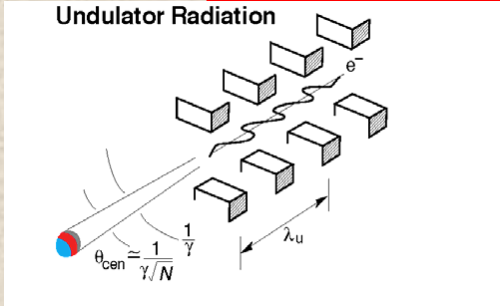
$$I = I_U(1 + K^2/2)/2g^2 \qquad K = eB_U I_U/2\rho mc^2 \gg 1 - 3$$

$$DI/I = 1/N_U$$

Number of coherent photons/electron $\quad aK^2/(1 + K^2) \gg 10^{-2}$

$N_u \lambda$
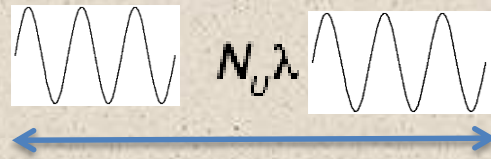
Disordered state: single electron wave trains superimpose with random phases: noise. **Intensity ~ N_e**
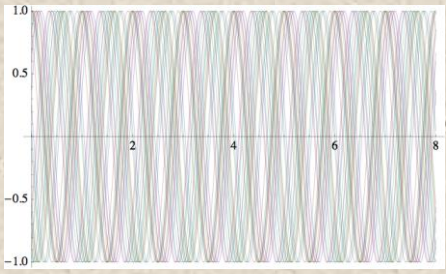
The FEL instability takes us from the disordered to an ordered state
Ordered state: wave trains superimpose in phase. **Intensity ~ N_e^2**

The order parameter is the "Bunching factor" $\quad B = \dfrac{1}{N_e} \sum_{1}^{N_e} \exp(iF_n),$

F_n is the relative phase of the wave and electron oscillation. *B=1* is perfect order.
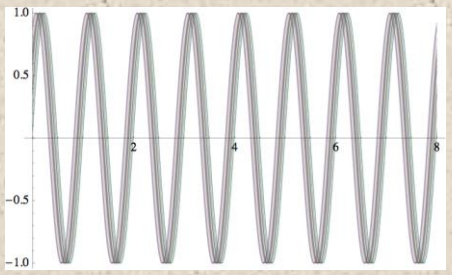
The FEL parameter

The instability is characterized by a single universal FEL parameter

$$r = \left(\frac{K W_P}{4 g w_U} \right)$$

Exponential gain length
$$L_G = \frac{l_U}{4 p r}$$

Saturation power
$$P_{FEL} = r P_{beam} = r I_{beam} E_{beam}$$

For the instability to develop, the electron beam must satisfy three conditions on its space phase density:

$s_r s_q \pounds l / 4 p$ Transverse phase space matching

$s_E < r$ Cold beam

$L_G < Z_R$ Gain> diffraction losses

Random   Well bunched
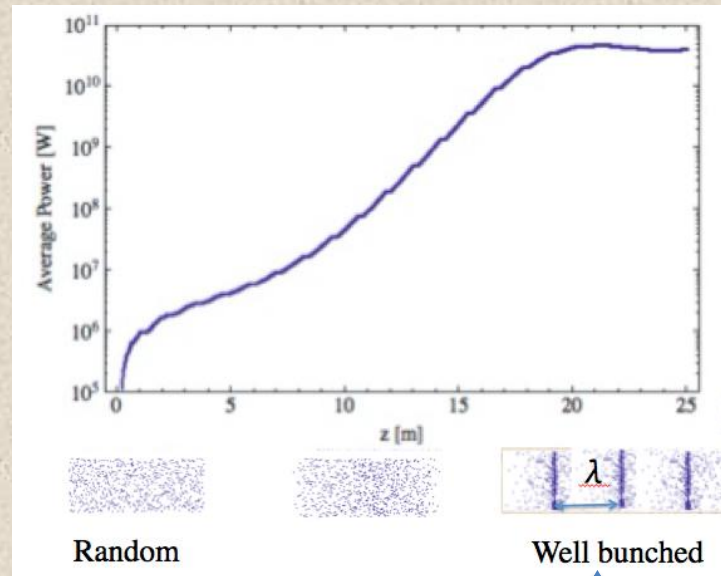
Initial beam state   Final beam state

LCLS Example: E_{ph}=10keV, E=15 GeV, ρ=10^{-3}. We obtain ~10^3 coherent photons/e.

(Compare to ~10^{-2} for spontaneous radiation). P_{FEL}~45 GW.

The LCLS
(Linac Coherent Light Source)

UCLA
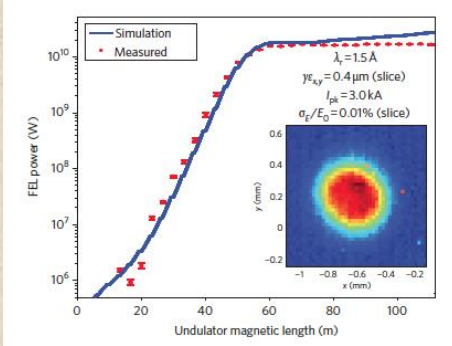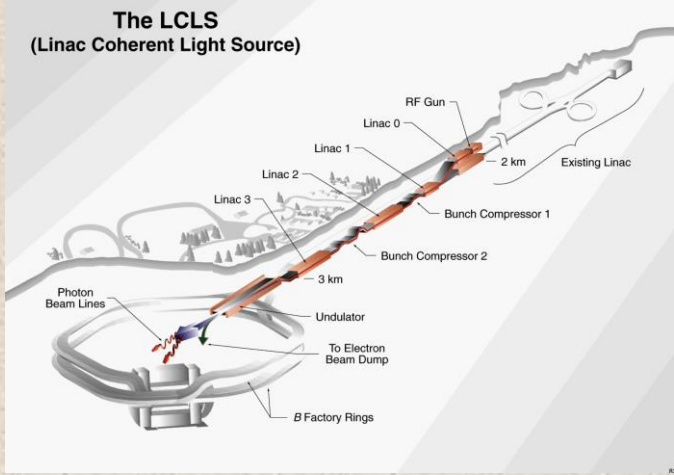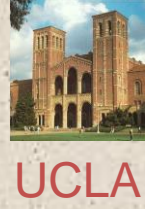
LCLS, 1.5 Å, 4/2009, 1-3 mJ
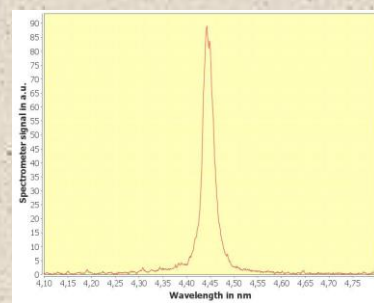
Flash: 4.45 nm, 0.3 mJ, 6/2010
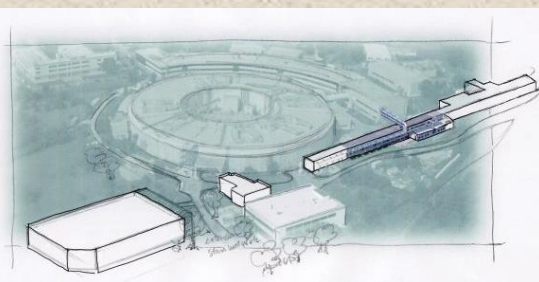
Fermi@Elettra, 43nm,12/2010

SACLA 0.8 Å, 6/2011
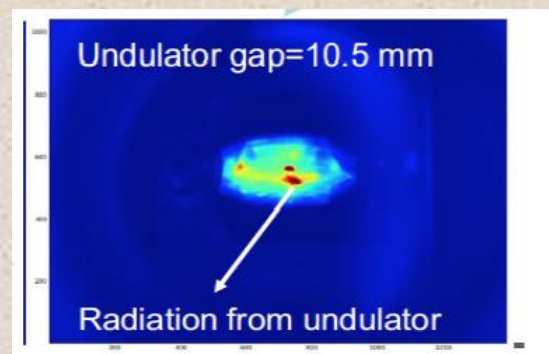
UV FEL Dalian, 50-150 nm, January 2017

Recently added hard X-ray FELs: Korean X-FEL (lased at 0.1 nm, 3/16,2017); European XFEL (lased at 0.15 nm, 6/23/2017)

4 GeV SC Linac

4 GeV, 0.3 mA, 1.2 MW

0.2-1.3 keV (120 kW)

SCRF Linac in 1st km of SLAC tunnel

Cu Linac

1.0 - 20 keV (120 Hz)
1.0 - 5 keV (120 kW)

LCLS-II

SXFEL Tunnel completion, April 2016
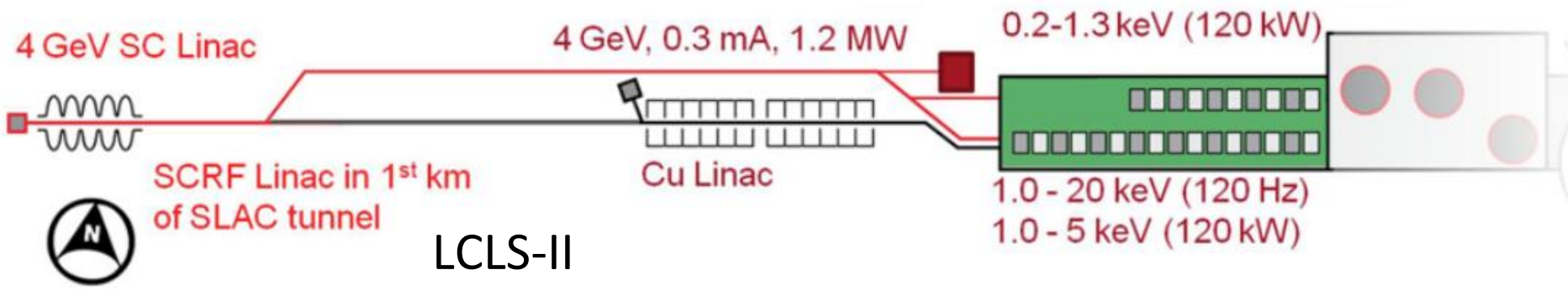
Shanghai SXFEL, S+C band, 1.6 GeV, 2-10 nm

1st Construction phase

2013-16

2nd construction phase

2017-20

Athos 0.7-5nm

user stations

2.7-3.3 GeV

Injector   BC1   Linac 1   BC2   Linac 2   Linac 3

0.35 GeV   2.1 GeV   3.0 GeV   2.1-5.8 GeV   Aramis 0.1-0.7 nm
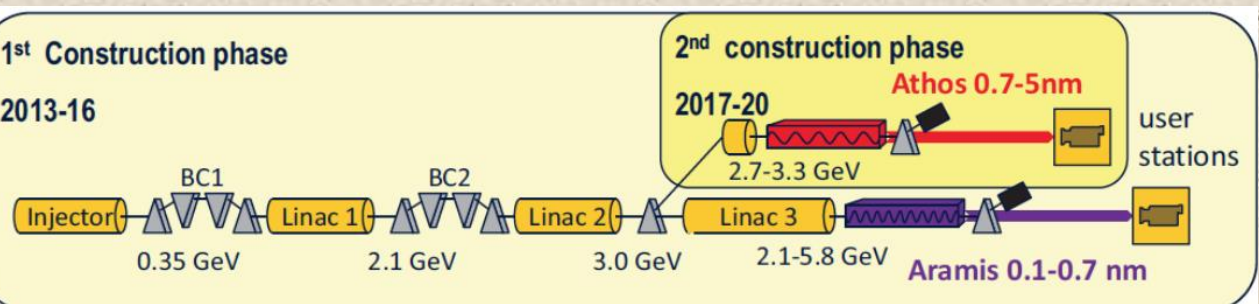
Swiss FEL0.1-5nm, 100 Hz, First lasing at 0.9 GeV, 4 nm, May 2017 .

Comparison of X-ray sources
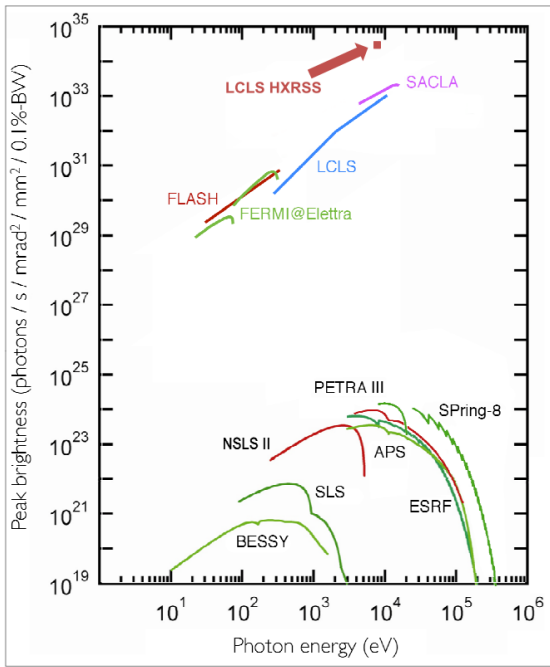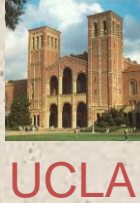
X-ray sources brightness (number of photons in the X-ray beam six dimensional phase space). In practical units it is the number of photons/sec/mm^{2}mrad^2/0.1% bandwidth. . Notice the jump by a factor 10^9 with LCLS in 2009.

Main XFELs characteristics

- Photon energy range: 10-0.1nm
- Peak power: 1-50 GW
- Line width: 10^{-3}-10^{-4}
- Pulse length: few-100 fs
- Repetition rate: 10^2-10^6 Hz
- Flexibility: high, the x-ray pulse can be tailored to the experiment
- Two colors with delay variable from few to 100 fs, or ns

LCLS: the world's first x-ray free electron laser

Injector

electron beam

1km linac 14GeV

Undulator hall

Near-hall: 3 stations

x-ray beam

6/24/2017

Far-hall: 3 stations
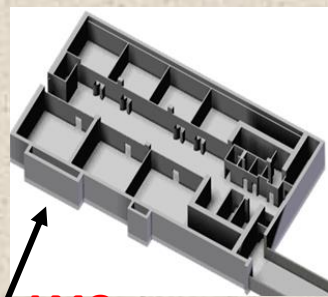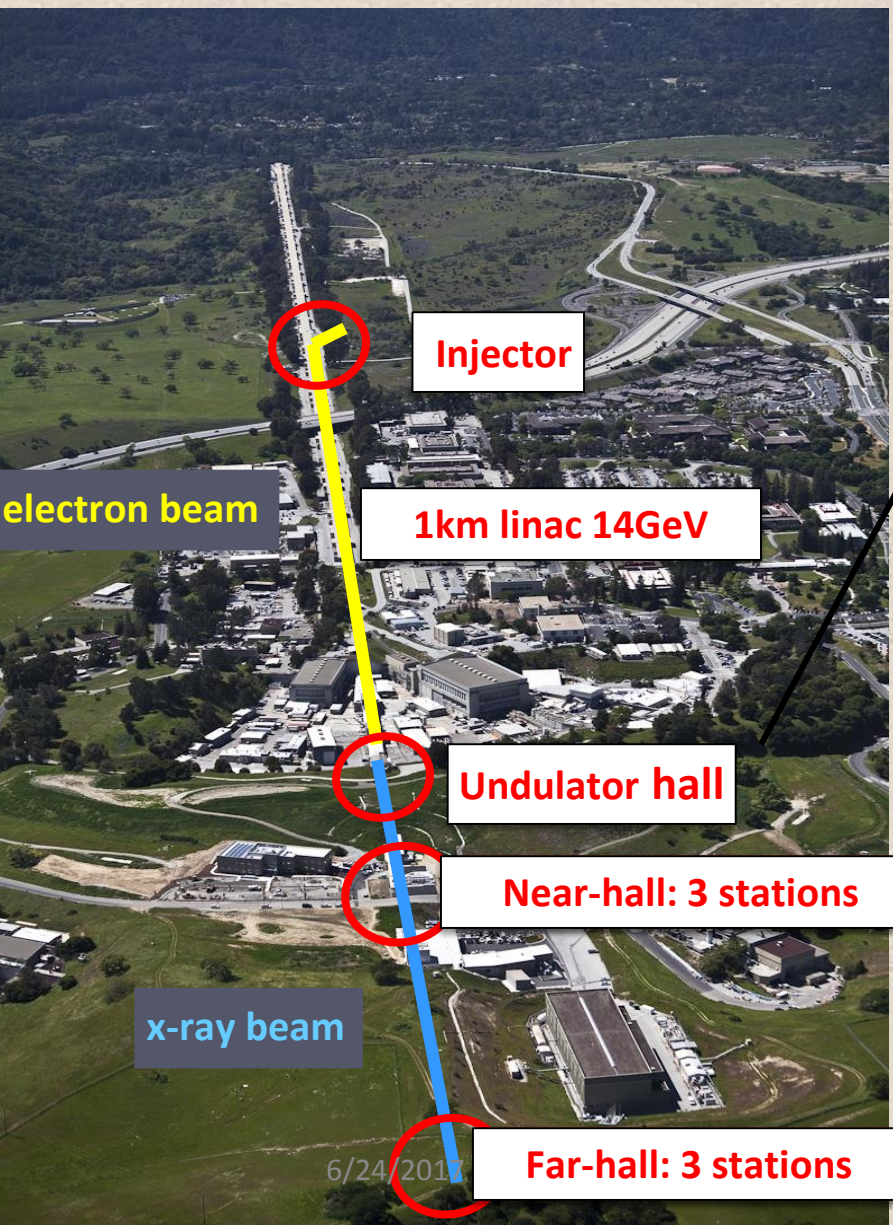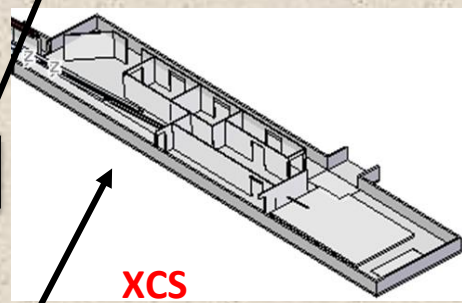
AMO: Atomic, Molecular & Optical Science
CXI: Coherent X-ray Imaging
MEC: Matter in Extreme Conditions
SXR: Soft X-ray Materials Science
XCS: X-ray Correlation Spectroscopy
XPP: X-ray Pump Probe

AMO **SXR** **XPP**

More instruments will be added with LCLS II, starting about 2018.

XCS

CXI **MEC**

C. Pellegrini, Passion for Physics

Coherence properties of X-ray FEL
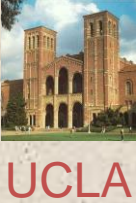
Transverse coherence: good.
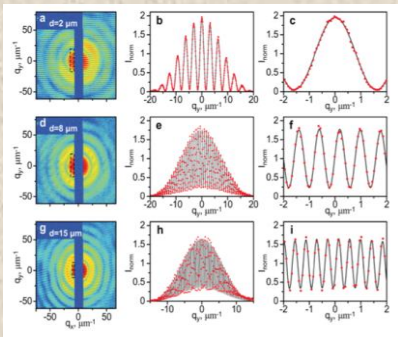
Coherence properties of individual femtosecond pulses of an X-ray FEL, I. A. Vartanyants et al., 2011, Phys. Rev. Lett. 107, 144801.

Improving LCLS temporal coherence: Self-seeded spectra

In a SASE FEL the spectrum is wide and fluctuates. Bonifacio, Pellegrini et al., Phys. Rev. Lett. 1994, **73**,70. Self-seeding is a way to improve the spectrum and reduce the line-width using the transmission around the stop band of a Bragg reflection in a diamond crystal, Geloni, G., V. Kocharyan and E. Saldin, 2011, J. of Mod. Opt. **58,** 1c
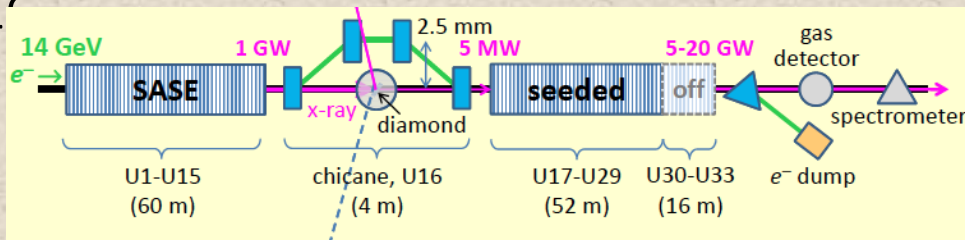
The concept as been demonstrated at LCLS , J. Amann, et al. Nature Photonics, DOI: 10.1038/NPHOTON 2012.180
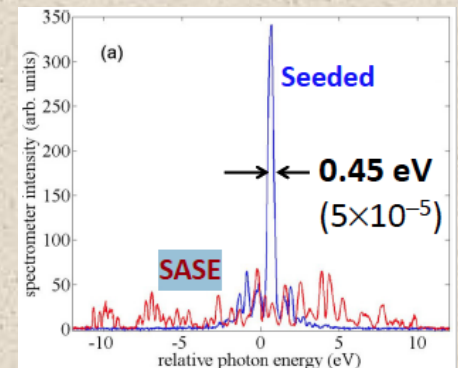
99% circular polarization with DELTA undulator
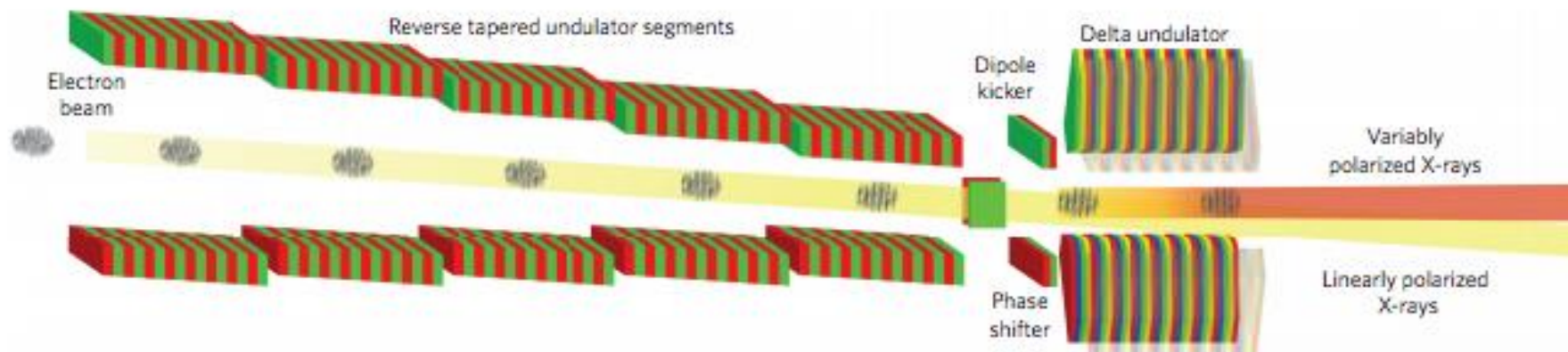
The beam is microbunched in a planar undulator with decreasing gap to suppress linearly polarized radiation. A dipole kicker redirects the beam into the
repointed Delta undulator. The Delta undulator produces arbitrarily polarized X-rays. A phase shifter controls the phase between the linearly polarized light at the entrance of the Delta and the microbunches in the electron beam.
Result: over 99% circular polarization.

➢ 100s of µJ in 10s of fs from 280-1200 eV
➢ Reverse taper improves polarization
➢ Undulator pointing separates polarization components
➢ Full circularly polarized X-rays within accuracy of measurement (98% -4%+2%).

A. A. Lutman et al., Polarization control in an X-ray free-electron laser, Natire Photonics, **10**, 468 (2016).

Manipulating the gain medium

For an X-ray FEL the gain medium is the electron bunch. Gain can be enhanced or switched off for the full bunch or part of it (a slice) in several ways:

1.   By making it oscillate around the undulator axis;

2.   By increasing the slice emittance or the energy spread;

3.   By creating a slice with a large peak current.

2-color fresh bunch lasing enabled by Dechirper

❑ Enable fresh lasing of two e-beam slices at different times/energies

❑ Used for 2-color, time-delayed X-ray pulses: *up to 1 mJ /pulse*

❑ Variable delay for pump-probe studies: *(-15 fs to 950 fs)*

XTCAV image

Two independently lasing portions
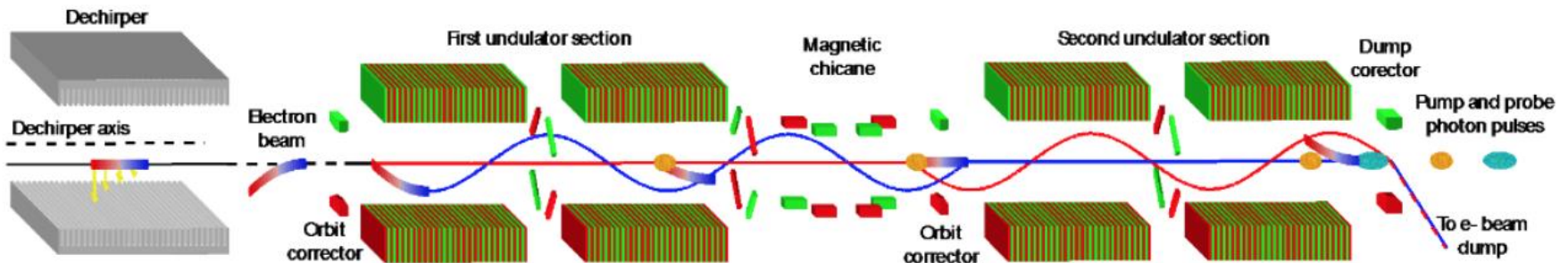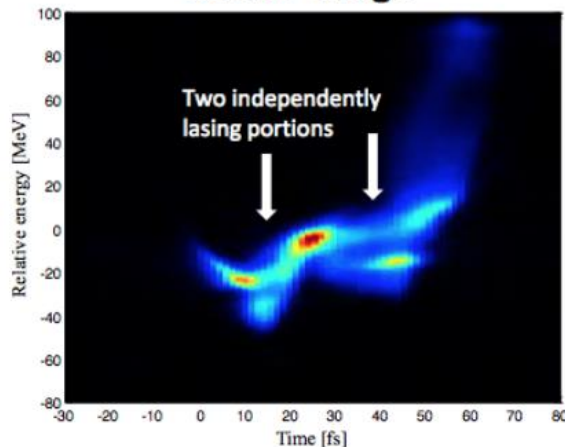
Two-color spectrum
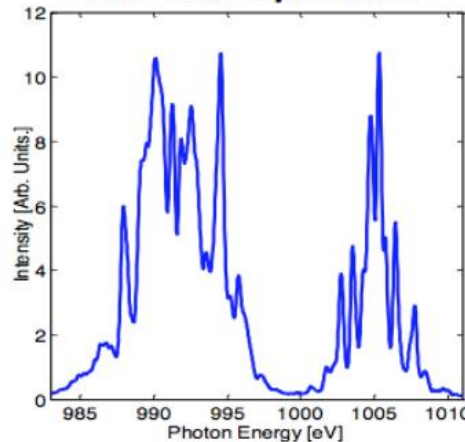
A. Lutman, T. Maxwell, et al., *Nat Photon*, **10**, 745 (2016)

Attosecond pulses: XLEAP
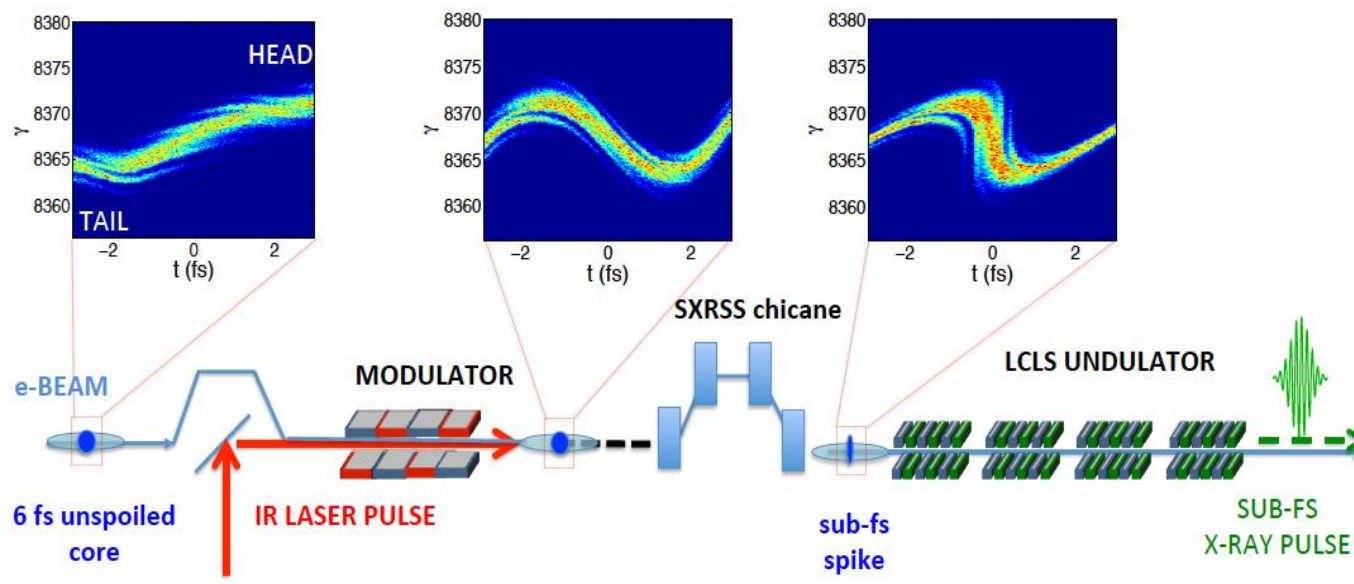
Enhanced SASE
Use intense IR pulse in a wiggler to compress a fraction of the electron beam.
(A. Zholents, 2005)

Courtesy A. Marinelli

ΔT = ~0.5 fs FWHM, E$_{pulse}$ ~ 20 to 50 uJ
-10 x shorter than fastest pulse measured at LCLS.
- 4 times shorter than typical cooperation length.
Coherent bandwidth ~ 5 eV
4 times larger than achieved before at SXR.
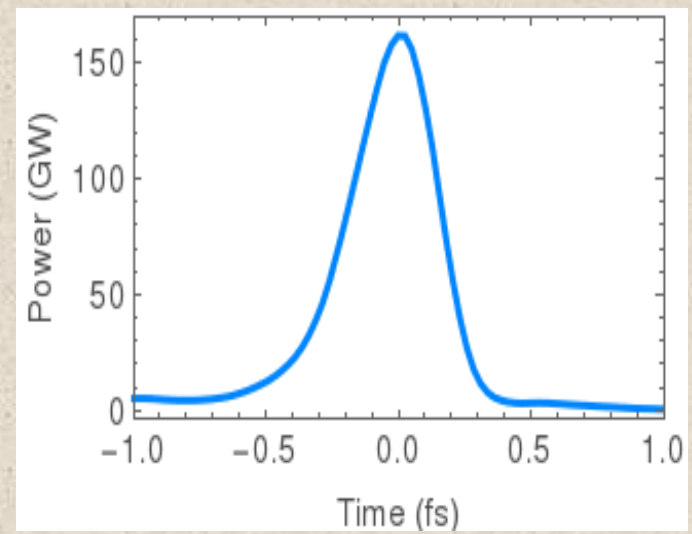
Attosecond Pump/Probe with Two-Color XLEAP

Variable delay

< 1 fs
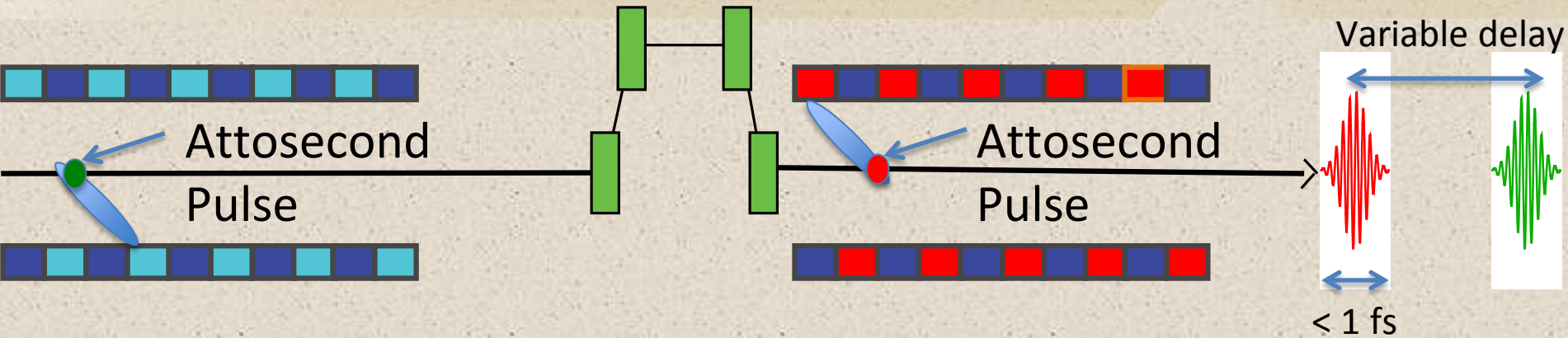
Use different e- beam spikes in two halves of the undulator.

Delay LOCKED by the laser modulation:
Two sub-fs pulses with sub-fs jitter!

$$\Delta T = \Delta T_{CHICANE} + N\lambda_{LASER} + Slippage$$

Courtesy A. Marinelli

XLEAP in combination with:
-time-dependent wake
(A. Lutman et al.)
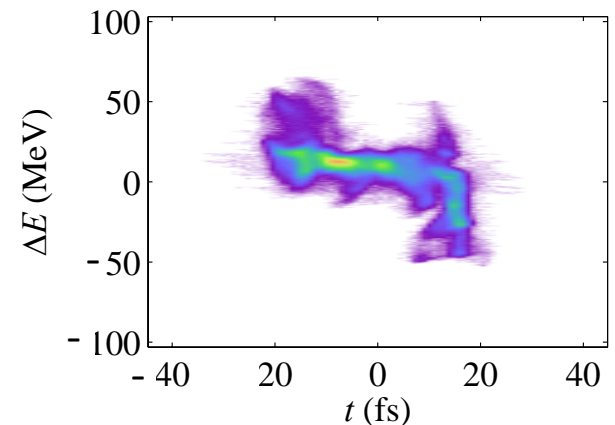
Toward High Power: The Double Bunch XFEL[*]

UCLA

Chicane

Seed generating FEL

High efficiency tapered amplifier

Monochromator
and X-ray delay

~ 1ns
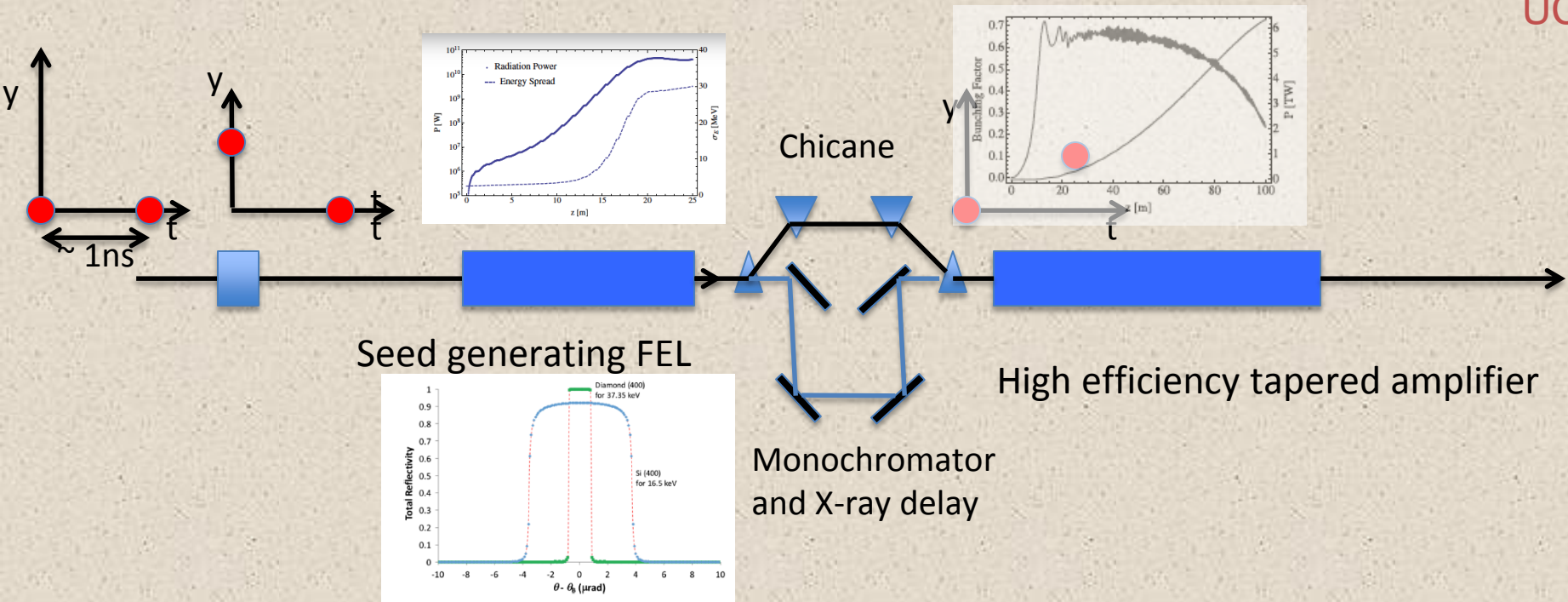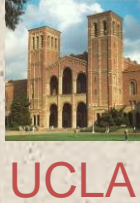
The DBFEL increases 100 times the efficiency of energy transfer, and the peak power. Operating LCLS with two bunches has already been demonstrated.[**]

[*]C. Emma, Y. Feng, D. Nguyen, A. Ratti, and C. Pellegrini, Phys. Rev. Acc. and Beams **20**, 030701 (2017).

[**]Characterization of the LCLS "nanosecond two-bunch" mode for X-ray Speckle Visibility Spectroscopy experiments, Y. Suna et al., SPIE 10237, 102370N-1-10 (2017).

UCLA

E_{photon} =5.5 keV, 2.2 Å
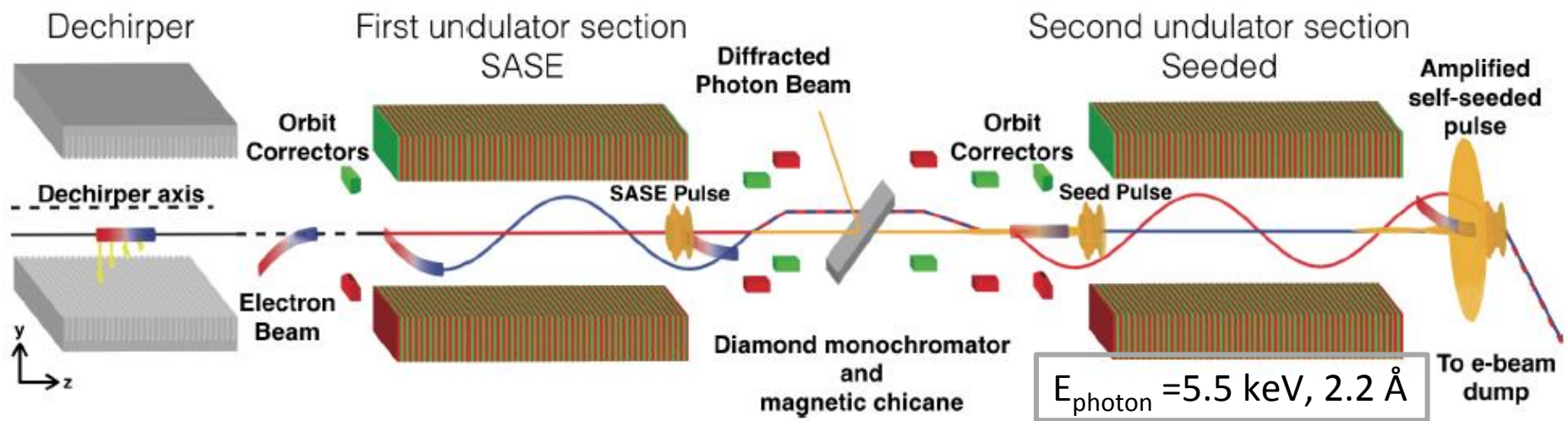
Schematic of the enhanced (fresh bunch) self seeding, ESS, experiment at LCLS. The bunch tail generates the seed signal in the first part of the undulator, where the head is oscillating and not lasing. After the monochromator the tail oscillates, the head moves on axis and amplifies the seed signal. The oscillation is generated by an off-axis dechirper and kickers.

Gain length change with oscillation kick:

$$L_G = L_{G0} / (1 - q^2 / q_C^2), \quad q_c = \sqrt{l / L_{G0}} \approx 10 \, mrad \text{ at } 1 \text{ nm}$$

*C. Emma, A. Lutman, M. W. Guetg, J. Krzywinski, A. Marinelli, J. Wu, and C. Pellegrini, Appl. Phys. Lett. **110**, 154101 (2017).

Experimental results

Measurements with X-band transverse cavity.

Top: Self seeded case; Single shot longitudinal phase space with, left, and without, middle, lasing; X-ray pulse energy 904 μJ, seeded pulse duration 29 fs, most of the electron beam contributing to lasing.

Bottom: Same plots in the ESS scheme. Lasing electrons in SASE section are on the tail (t = 20 fs); seeded electrons in the core (t = 0) have large energy loss $\sim$ 90 MeV. Peak X-ray power 50 GW, FWHM pulse duration 9 fs. Error bars calculated using the combined rms intensity error of two independent detector readings.
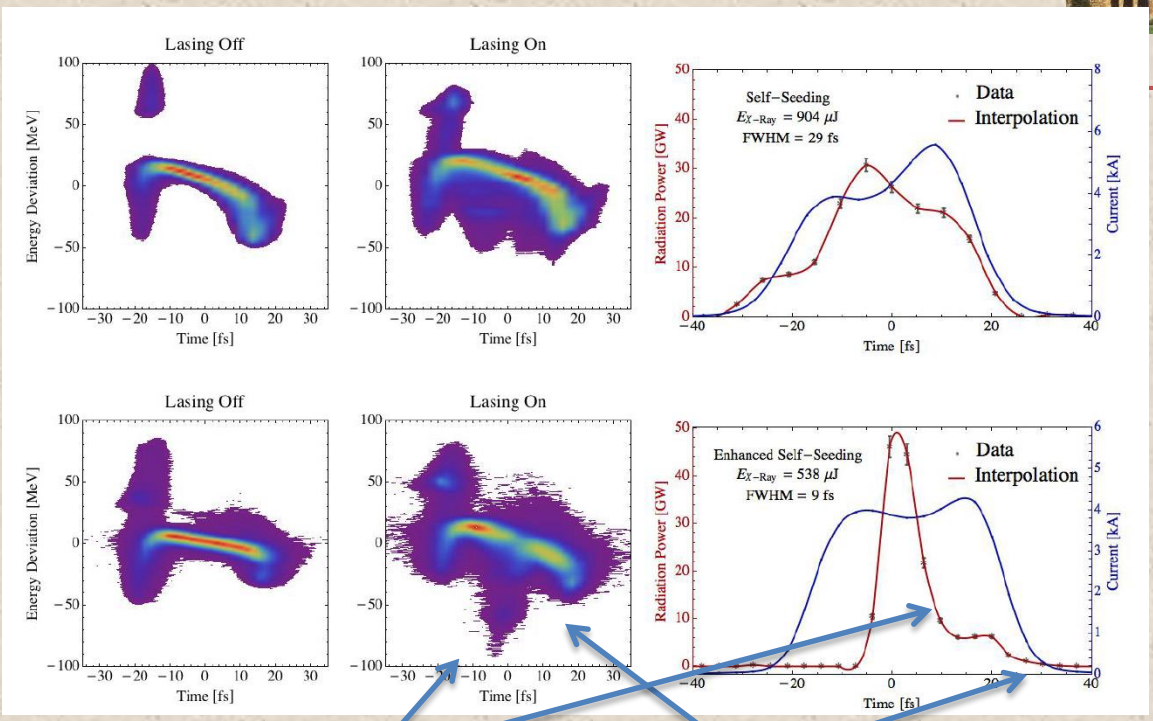
Seeded core

SASE lasing slice

ESS (fresh slice self seeding) generates 3 times shorter pulses with higher peak power.

With LCLS-II copper linac, an Advanced Undulator and the double bunch system we can reach 6TW peak power in 100 m at photon energy of 10 keV [*].
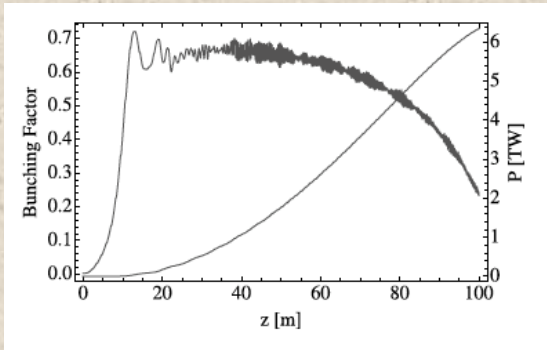
Power density and peak electric field:
$W = 3 \times 10^{23}$ W/cm^2, $E = 10^{15}$ V/m at 10 nm spot size

[*]C. Emma, Y. Feng, D. Nguyen, A. Ratti, and C. Pellegrini, Phys. Rev. Acc. and Beams **20**, 030701 (2017).

UCLA
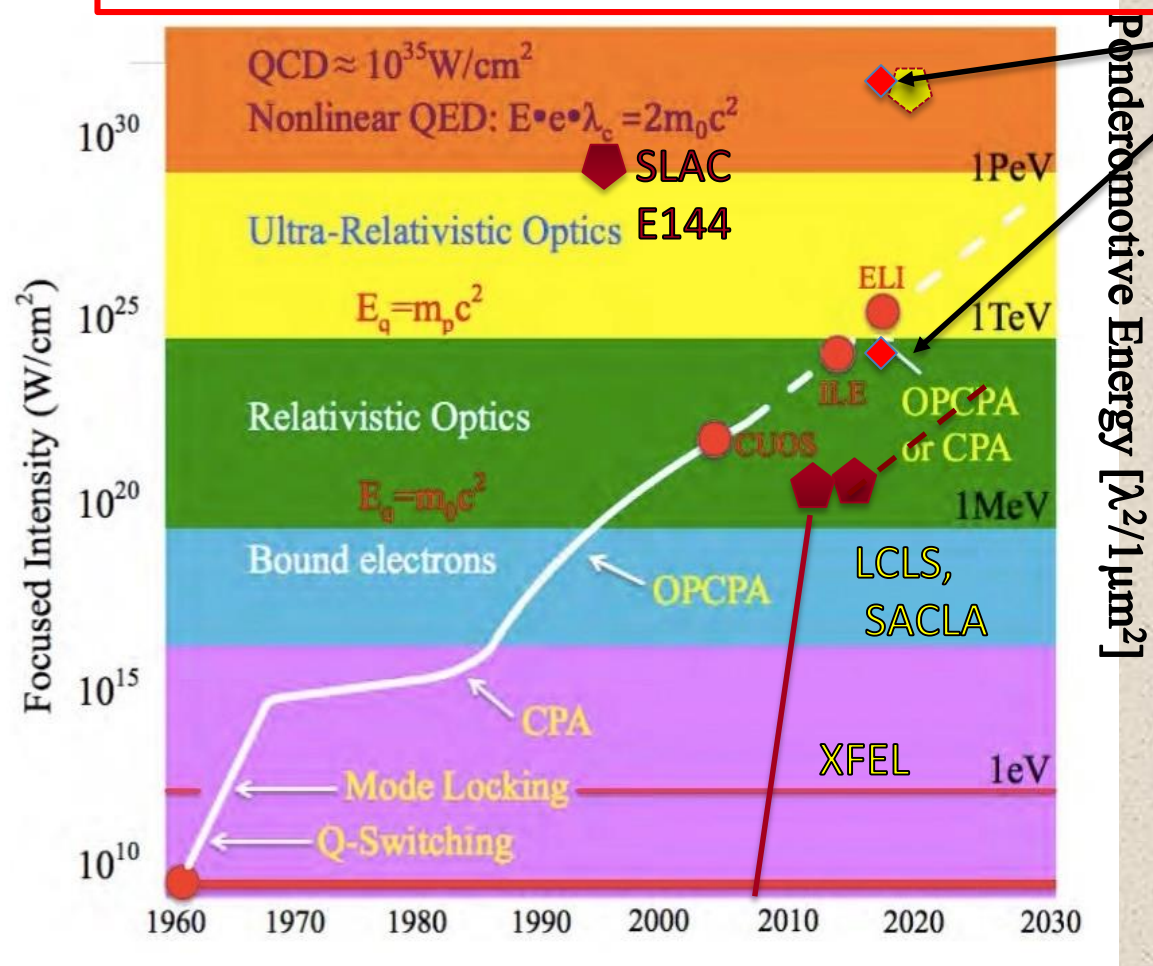
LCLS-II e-γ ≈10^{33} W/cm^2
LCLS-II ≈$3×10^{23}$ W/cm^2

$QCD \approx 10^{35} W/cm^2$
Nonlinear QED: $E \cdot e \cdot \lambda_c = 2m_0 c^2$

SLAC
E144

Ultra-Relativistic Optics

$E_q = m_p c^2$

ELI

1PeV

1TeV

Relativistic Optics

$E_q = m_0 c^2$

ILE

OPCPA or CPA

CUOS

1MeV

Bound electrons

OPCPA

LCLS, SACLA

XFEL

1eV

Mode Locking

Q-Switching

Ponderomotive Energy [λ^2/1μm^2]

Focused Intensity (W/cm^2)

- New strong-field and collective phenomena only accessible above QED critical intensity/field
- Current and future light sources far from this limit.
- Only possible by combining high energy particles with laser (relativistic boost)

  - $4\gamma^2$ intensity
  - 2γ field

Modified from https://eli-laser.eu/media/1019/eli-whitebook.pdf

Conclusion: X-ray FELs today and tomorrow

XFEL characteristics:	Today	Tomorrow
Wavelength, nm	10-0.1	10-0.01
Transverse coherence	good	good
Line width	10^{-3}-10^{-4}	10^{-2}-10^{-6}
Peak Intensity, mJ	2-4	2-100
Pulse duration, fs	100-4	100-0.3
Peak Power, TW	0.02-0.05	1-10-100?

Peak intensity and power can be increased by a factor 10 to 100 using tapered undulators and multi-bunch techniques.

… and the day after tomorrow

Plasma wakefield accelerator
Energy 2-12 GeV
$I_{peak} > 10kA$
Normalized emittance $< 10^{-7}m$
Energy spread $< 10^{-3}$

Advanced undulator
1-2 cm period
Gain length 10-40 cm

X-rays photon energy 0.5-100 keV
Peak power 0.01-10 T
Pulse duration 0.1-100fs

< 30 m

Imaging Molecular Motion: Femtosecond X-Ray Scattering of an Electrocyclic Chemical Reaction

M. P. Minitti,[1,*] J. M. Budarz,[1,2] A. Kirrander,[3] J. S. Robinson,[1] D. Ratner,[1] T. J. Lane,[1,4] D. Zhu,[1]
J. M. Glownia,[1] M. Kozina,[1] H. T. Lemke,[1] M. Sikorski,[1] Y. Feng,[1] S. Nelson,[1] K. Saita,[3] B. Stankus,[2]
T. Northey,[3] J. B. Hastings,[1,†] and P. M. Weber[2,‡]

UCLA
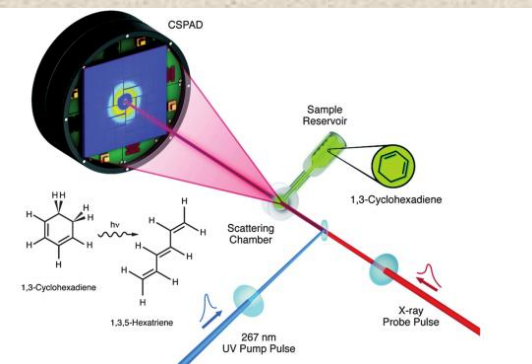
8.3 keV, 30 fs, 10^{12} photons/pulse, 3 torr
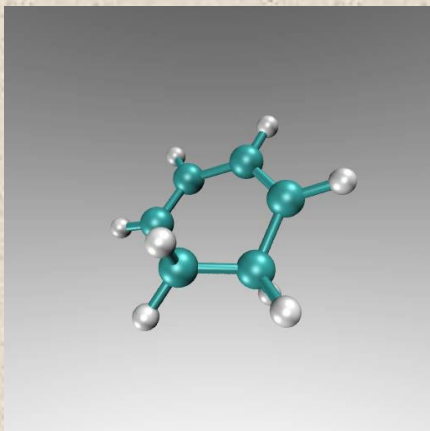
Reaction movie in 30 fs.

… .. By mapping nuclear motions using femtosecond x-ray pulses, we have created real-space representations of the evolving dynamics during a well-known chemical reaction and show a series of time- sorted structural snapshots produced by ultrafast time-resolved hard x-ray scattering.

Our analysis shows that, upon absorption of the optical photon, the chemical reaction of 1,3-cyclohexadiene to 1,3,5-hexatriene starts with a rapid expansion of the carbon bonds of the cyclohexadiene ring. ..

Within one or two oscillations of the carbon skeleton, the C1–C6 chemical bond breaks as the terminal carbon atoms move perpendicular to the molecular plane along the reaction coordinate. It is already at this point that the terminal hydrogen atoms of the nascent hexatriene molecule align to conform to the Woodward-Hoffman rules. Consequently, the stereochemical fate of the chemical reaction is sealed as early as 30 fs after the optical excitation.

Molecular movies 2
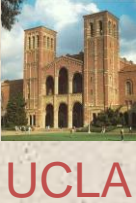
UCLA
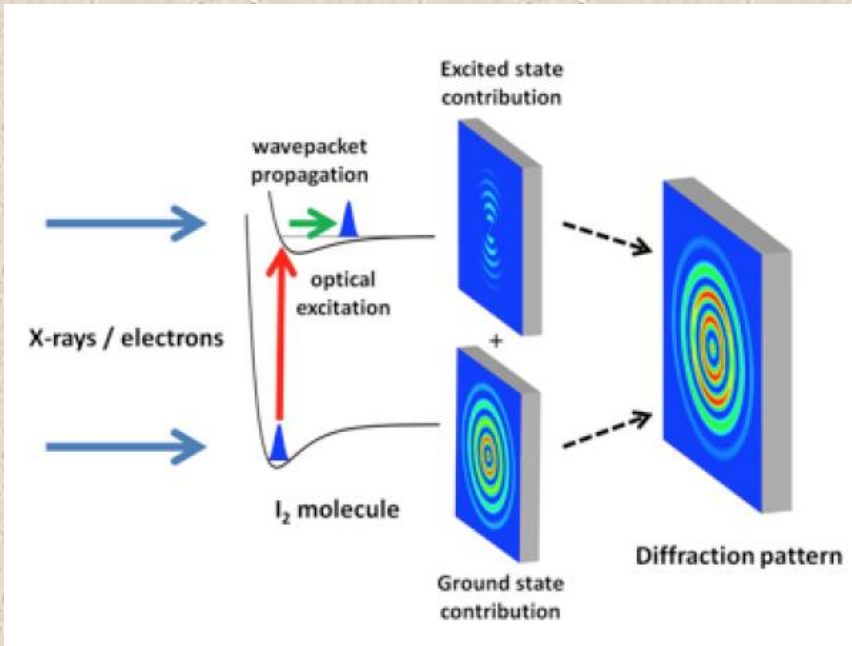
''Molecular movie'' showing the vibration of an iodine molecule triggered by the excitation to a low-lying electronic state. Diffraction patterns are measured using an ultra short x-ray pulse with variable delay from LCLS X-FEL. The vibrational motion is extracted by unfolding the holographic interference between x rays scattered from ground-state molecules and x rays scattered from vibrationally excited molecules.
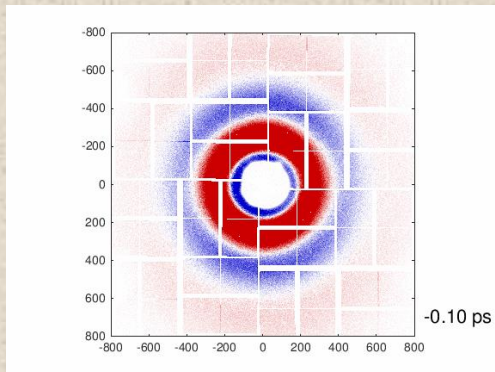
9.0 keV, 2 mJ, 120 Hz, 40 fs, horizontal polarization, 30 μm beam diameter.

Raw data as a function of pump-probe delay. The average scattering image over all time delays is subtracted to show more easily the interference features.

Molecular movies
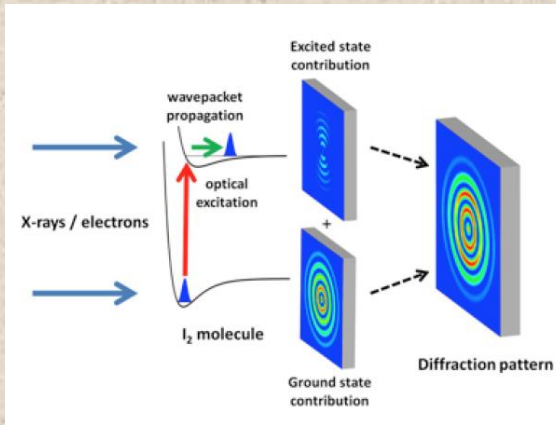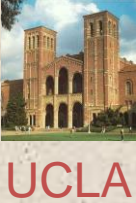
X-ray spatial coherence is required for this experiment.

The experiment image, in real time, the changes of the distance between the two atoms in a vibrating iodine molecule. The x-ray scattering signal is the mixing of two contributions. The first comes from the fraction of molecules in the gas sample excited by the visible pump laser (typically 1–10%). These molecules are displaying a vibrational wave-packet motion and produce a weak x-ray scattering pattern that, by itself, is not measurable. However, this signal becomes measurable through its interference with the stronger x-ray scattering pattern from the ground-state molecules. By subtracting a ground-state-only scattering pattern (measured when the x-ray probe precedes the visible pump), the authors isolate the ground-state and excited-state interference contribution to the signals. The internuclear distance is obtained from the interference pattern formed by the ground-state and excited-state signals.

The analysis does not rely on molecular modeling and shows oscillations in the internuclear distance of the vibrational wave packet with a period of a few hundred femtosecond and a space/time resolution of 0.3A/30fs.
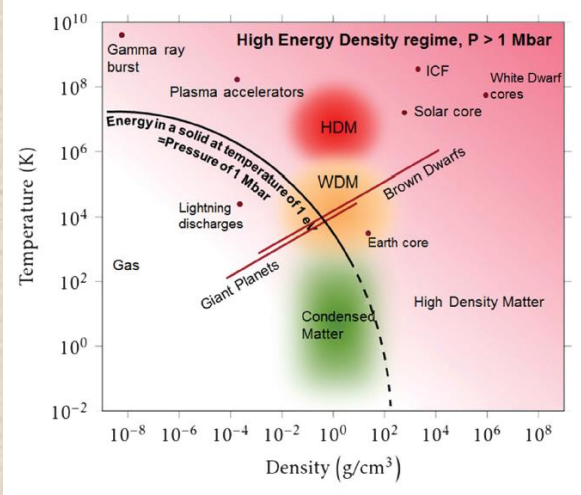
Map of high-energy density (HED) regime above 1 Mbar. HED science includes study of warm dense matter (WDM), hot dense matter (HDM), interior of planets, astrophysics, relativistic laser plasmas, inertial confinement fusion.

Many experiments with LCLS to irradiate a solid density sample and measure subsequent K-shell emission of dense aluminum plasmas, revealing saturation of the absorption induced by the ionization in the x-ray regime (Rackstraw et al., 2015) and much larger lowering of the ionization potential (Cho et al., 2012; Ciricosta et al., 2012; Vinko et al., 2012, 2015; Vinko, Ciricosta, and Wark, 2014) than predicted by commonly used plasma models (Stewart and Pyatt, 1966).
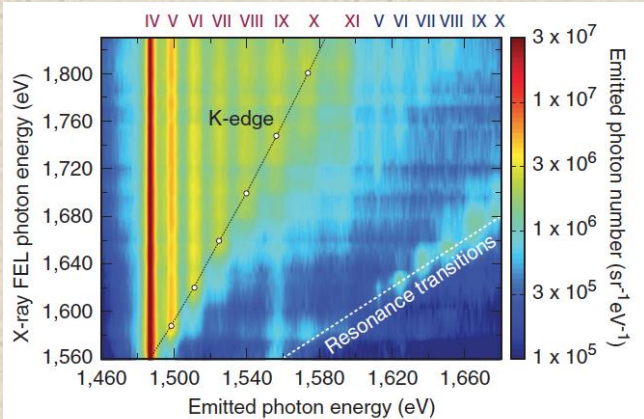
Vinko, S. M., et al., 2012, Nature **482**, 59; and 2015, Nat. Commun. **6**, 6397.

Spectrally resolved Al Kα emission as a function of x-ray FEL excitation photon energy from 1460 to 1680 eV. Emission lines from Al charge states from 4. to 10. are marked in Roman numerals: red for states with a single K-shell hole and blue for states with a double K-shell hole.

Chung, Ciricosta, Falcone, Heimann, Lee, Nagler, Vinko, Wark received the 2015 APS Dawson Prize for creating high density plasma, measure ionization potential depression with X-ray FEL and new theories to explain discrepancies with old models.

X-ray FELs impact on structural biology

Biophysical Highlights from 54 Years of Macromolecular Crystallography

Jane S. Richardson* and David C. Richardson
Biochemistry Department, Duke University, Durham, North Carolina

ABSTRACT   The United Nations has declared 2014 the International Year of Crystallography, and in commemoration, this review features a selection of 54 notable macromolecular crystal structures that have illuminated the field of biophysics in the 54 years since the first excitement of the myoglobin and hemoglobin structures in 1960. Chronological by publication of the earliest solved structure, each illustrated entry briefly describes key concepts or methods new at the time and key later work leveraged by knowledge of the three-dimensional atomic structure.

54. Free-electron laser crystallography

Free-electron laser crystallography is without question the most spectacular new technical development in the field. A jet of droplets with nanocrystals is sent past a beam of femtosecond x-ray laser pulses, and diffraction is recorded before the crystal has time to explode. This has the potential for determining otherwise intractable molecular structures and for accessing rapid time steps. The many challenging problems with data and analysis appear to be solvable. After demonstration structures of photosystems and lysozyme (e.g., PDB:3PCQ (126), PDB:4FBY (127), PDB:4ET8 (10)), there is now a novel structure of propeptide-inhibited trypanosomal cathepsin B (PDB:4HWY (128)) potentially useful for drug design. (Fig. 54. Cα splines and chromophores (*pink*) in Photosystem II (PDB:4FBY)).
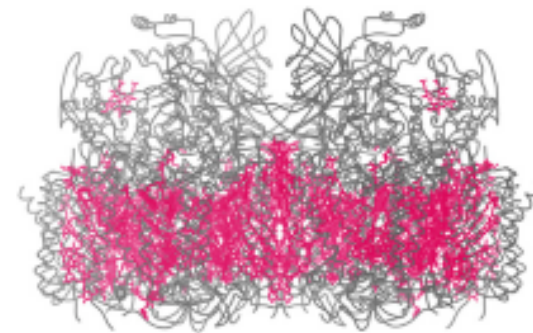
Henry Chapman received the 2015 Leibniz Prize for this work

Natively Inhibited Trypanosoma brucei Cathepsin B Structure Determined by Using an X-ray Laser, L. Redecke et al. Science 339, 227 (2013)
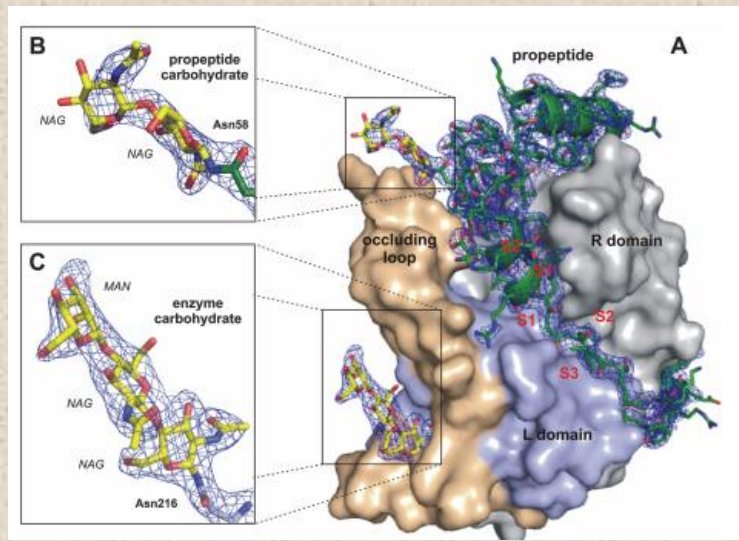
The Trypanosoma brucei cysteine protease cathepsin B (TbCatB), which is involved in host protein degradation, is a **promising target to develop new treatments against sleeping sickness, a fatal disease caused by this protozoan parasite.** …

By combining two recent innovations, in vivo crystallization and serial femtosecond crystallography, we obtained the room-temperature **2.1 angstrom resolution structure** of the fully glycosylated precursor complex of TbCatB. The structure reveals the mechanism of native TbCatB inhibition and demonstrates that new biomolecular information can be obtained by the **"diffraction-before-destruction"** approach of x-ray free-electron lasers from hundreds of thousands of individual microcrystals.

Times resolution: few femtosecond, few x 10^{-15} s.
In these measurements the time and space resolution are the atomic space and time scales.

Three-Dimensional Reconstruction of the Giant Mimivirus UCLA Particle with an X-Ray FEL. T. Ekberg et al., PRL 114, 098102, 2015

X-ray FELs such as LCLS can provide a path to single-particle imaging (SPI) by collecting 2D coherent diffractive imaging patterns from individual noncrystalline particles and assembling a three-dimensional pattern from multiple copies of sufficiently identical particles. The promise of single-particle imaging is tantalizing, with all the challenges related to crystal growth and crystallography in general removed. Studying single molecules free of the crystal contacts and interactions that may distort their structure at room temperature would be revolutionary. The extremely weak signal, especially at high resolution, expected from single biological molecules makes imaging them in this way very challenging.

T. Ekeberg et al. [1]

(Top) 24 of the 198 diffraction patterns collected by a sequence of single viruses injected into the XFEL beams. Each pattern comes from a virus with random orientation with respect to the x-ray beam. (Bottom, left) Through a mathematical algorithm, the orientation of each single-virus diffraction pattern was recovered and the 198 patterns were combined into a complete three-dimensional pattern. (Bottom, right) 3D electron density of the mimivirus recovered from such diffraction pattern. The achieved spatial resolution is 125 nanometers.
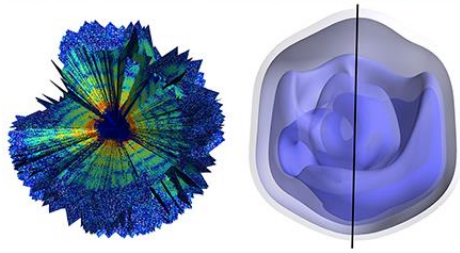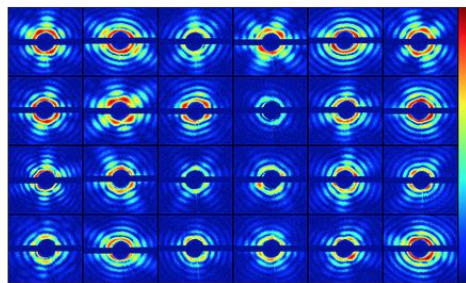
# De novo phasing with X-ray laser reveals mosquito larvicide BinAB structure, J.P. Colletier et al, Nature 2016, **539**, 43

A collaboration between UCLA, UCR, LBNL, Univ. of Grenoble, Stanford and SLAC.

UCLA
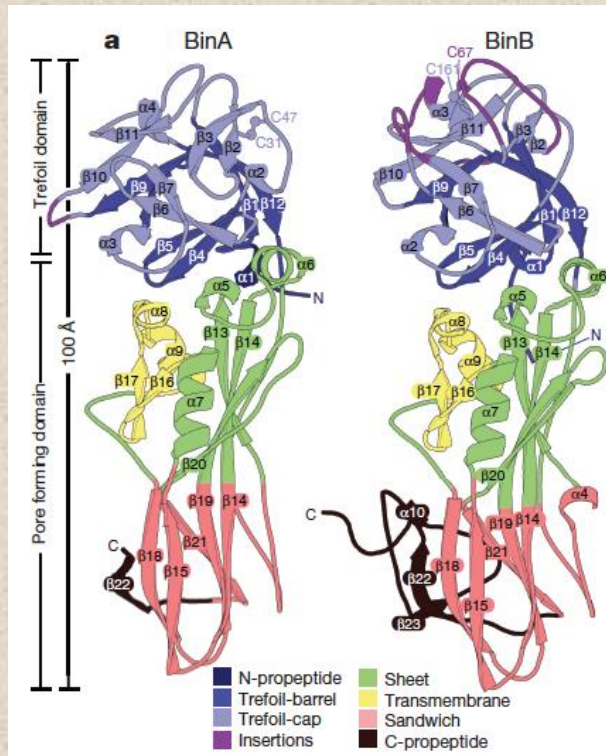
Countries around the globe have begun killing mosquito larvae using a natural toxin derived from bacteria. In this experiment X-rays from LCLS are used to determine the atomic structure of this larvicide, lethal to mosquitoes transmitting malaria and West Nile virus. These results reveal how the toxin functions, knowledge that will inform future efforts to genetically engineer it, to also kill mosquitoes carrying Zika virus and dengue fever.

BinA and BinB are structurally similar to each other, each composed of trefoil and pore-forming domains. The most noticeable differences correspond to insertions in surface loops on the trefoil domains (purple).
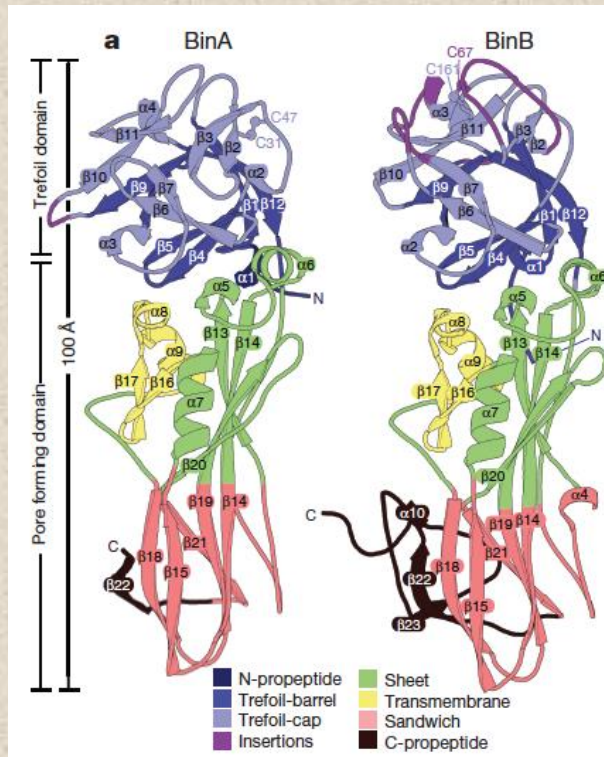
Naturally occurring protein crystals from Bacillus thuringiensis subsp. israelensis (Bti) and L. sphaericus are one of the most environmentally safe and efficient means of controlling mosquitos. The specificity and efficiency of the L. sphaericus binary toxin, BinAB, presumably arise from its structural complexity, which allows it to navigate through a series of barriers en route and recognize only its intended target.

The experiment elucidates the structure of BinAB crystals, revealing features that endow BinA and BinB with their functions. The authors suggest a mechanism by which alkalinity and proteolytic activation trigger a series of structural rearrangements that navigate BinAB past barriers to reach its target while maintaining the resilient 1:1 association throughout the life cycle.

UCLA

Angiotensin Receptor (AT1R)

Zhang H et al. 2015 Structure of the Angiotensin receptor revealed by serial femtosecond crystallography, Cell **161** 833
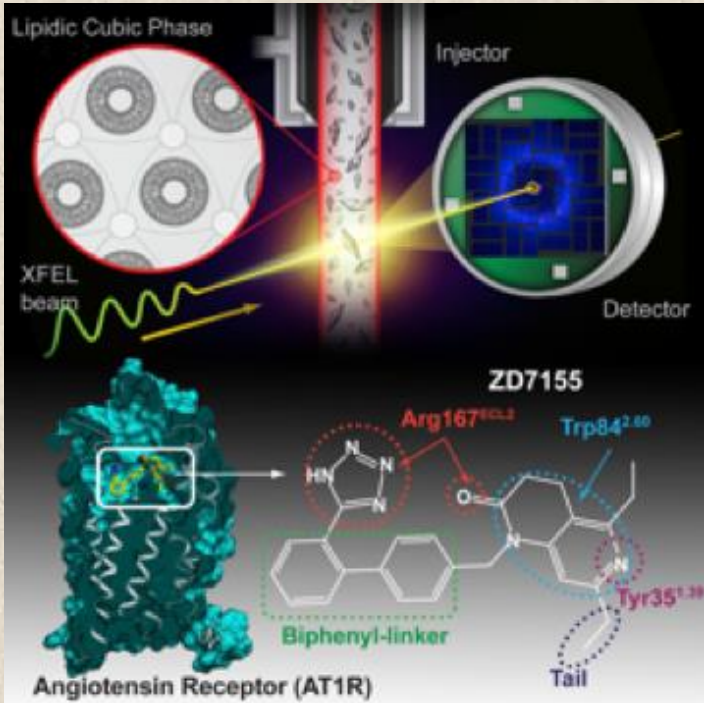
Angiotensin II type 1 receptor (AT1R) is a G protein-coupled receptor that serves as a primary regulator for blood pressure maintenance. Although several anti-hypertensive drugs have been developed as AT1R blockers (ARBs), the structural basis for AT1R ligand-binding and regulation has remained elusive, mostly due to the difficulties of growing high-quality crystals for structure determination using synchrotron radiation. Using serial femtosecond crystallography at an X-ray free-electron laser, we successfully determined the room-temperature crystal structure of the human AT1R in complex with its selective antagonist ZD7155 at 2.9-Å resolution. The AT1R-ZD7155 complex structure revealed key structural features of AT1R and critical interactions for ZD7155 binding. Docking simulations of the clinically used ARBs into the AT1R structure further elucidated both the common and distinct binding modes for these anti-hypertensive drugs. The results provide fundamental insights into AT1R structure-function relationship and structure-based drug design.

Exploring Vibration Modes in Gold Nanocrystals

Ultrafast Three-Dimensional Imaging of Lattice Dynamics in Individual Gold Nanocrystals, J. N. Clark et al., Science, 341, 6141 (2013)
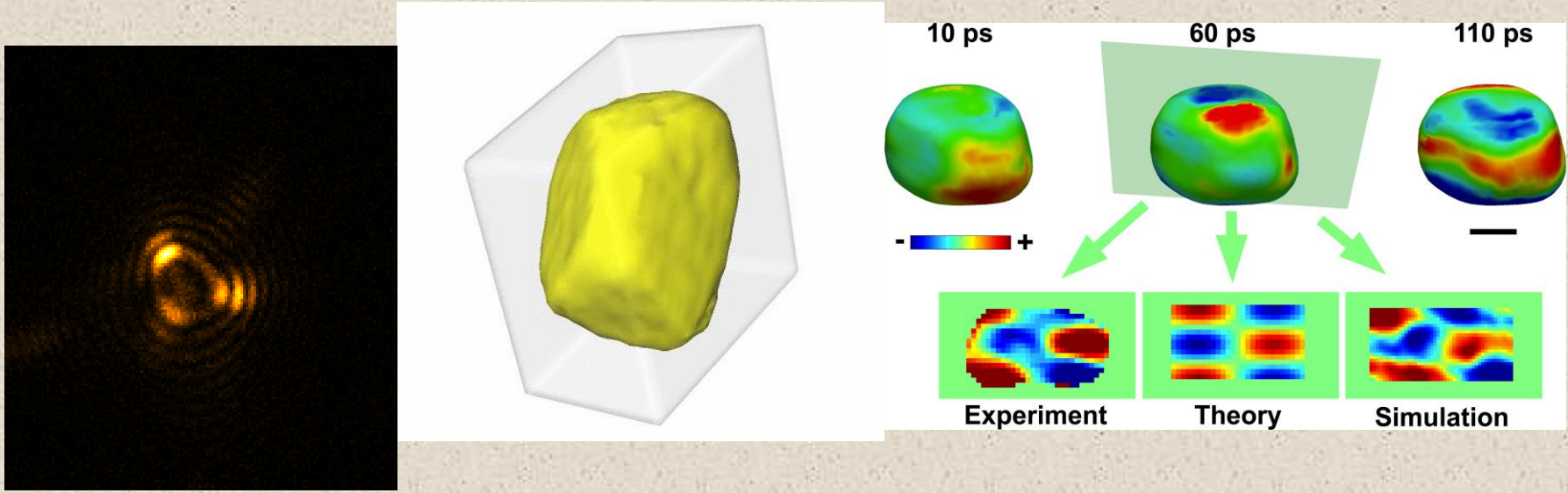
Key insights into the behavior of materials can be gained by observing their structure as they undergo lattice distortion.

Acoustic vibrations in gold nanocrystals (300-400 nm) triggered with infrared light pulses

- High-resolution real-space images of the deformation field inside the nanocrystal were obtained via the Bragg coherent diffraction imaging technique at various time delays
- Technique can extend to nanoscale objects of importance to catalysis and energy storage